JOURNAL OF MATERIALS SCIENCE 21 (1986) 2462–2474

Toughening mechanisms in elastomer-modified epoxies

Part 1 *Mechanical studies*

A. F. YEE*, R. A. PEARSON‡
Polymer Physics and Engineering Branch, Corporate Research and Development, General Electric Co., Schenectady, New York 12301, USA

Some brittle epoxies can be toughened significantly by the addition of an elastomeric phase. A great deal of controversy still exists on the nature of the toughening mechanisms. In this work tensile dilatometry at constant displacement rates was used to determine whether voiding, crazing or shear banding are the deformation mechanisms. Diglycidyl ether–bisphenol A epoxies toughened by various levels of several types of carboxyl-terminated butadiene nitrile liquid rubber were studied. The results indicate that at low strain rates the rubber particles simply enhance shear deformation. At sufficiently high strain rates the rubber particles cavitate and subsequently promote further shear deformation. No indication of crazing as an important toughening mechanism is found. No significant effect of rubber particle size or type can be ascertained.

1. Introduction

It is well known that some brittle epoxies can be toughened by an order of magnitude by the addition of a rubbery phase, yet a great deal of controversy still exists on the nature of the toughening mechanisms. Much of the dispute surrounds the issues of whether the rubber [1–3] or the matrix [3–11] absorbs most of the energy, and whether the matrix undergoes massive crazing [4, 5, 10, 11] or simple voiding [3, 6–9]. Presumably, once the mechanisms responsible for the increased toughness are clearly identified, then the material parameters responsible for these mechanisms can be enhanced or modified to produce an optimal combination of properties.

Several principal mechanisms have been proposed to account for the toughnes of these epoxies and are briefly reviewed here.

1.1. Toughening by crazing

McGarry and co-workers [4, 5] found that small ($< 0.1\ \mu m$) rubber particles did not toughen epoxies, whereas large (1 to 22 μm) particles increased the fracture toughness (measured as the strain-energy release rate, G_{Ic}) by at least an order of magnitude. In studying the biaxial yield behaviour of these epoxies, Sultan and McGarry [5] found that the yield criterion could be expressed in a modified Von Mises form:

$$\tau_{oct} = \tau_0 - \mu P \qquad (1)$$

where τ_{oct} is the octahedral shear stress, τ_0 is the critical octahedral shear strength of the material, P is the mean hydrostatic pressure and μ is the pressure coefficient. μ is > 0 and expresses the sensitivity of the material to the hydrostatic stress component. For both an unmodified epoxy and an epoxy modified by a highly soluble carboxyl-terminated butadiene nitrile rubber (CTBN), which resulted in small (40 nm) particles, μ was found to be 0.175. However, for an epoxy modified by a less soluble CTBN rubber, which resulted in large (1.2 μm) particles, two pressure coefficients were necessary to describe the failure locus: $\mu = 0.210$ in the first (tension–tension) quadrant, and $\mu = 0.175$ in the rest of the biaxial stress field. This result, together with the stress-whitening observed in the first quadrant, suggested to them that microcavitation at the crack tip was the toughening mechanism. They identified this microcavitation as crazing. This mechanism was cited by several workers [12, 13] to explain the toughness of other rubber-modified epoxies.

Stress-whitening can be caused by voiding as well as crazing [14, 15]. Simple voiding of or around the rubber particles could also have produced the increased pressure coefficient (larger μ) observed. Studies on other rubber-modified systems show that voiding and crazing result in very similar macroscopic biaxial tensile failure behaviour [16]. It can be argued that if the yield behaviour observed by Sultan and McGarry is due to crazing, then a crazing criterion, such as the one proposed by Sternstein and Ongchin [17], would have described the data more closely. Unfortunately, the scatter in the data is such that either of the two criteria mentioned above can describe the first-quadrant data equally well. The micrographic evidence by these workers [4, 5, 12, 13]

*To whom correspondence should be addressed. *Present address*: Department of Materials Science and Engineering, University of Michigan, Ann Arbor, Michigan 48109, USA.
‡*Present address*: General Electric Plastics Europe, PO Box 117, 4600 AC Bergen op Zoom, The Netherlands.

0022–2461/86 $03.00 + .12

supports the idea that simple voiding in or around the rubber particles is a major deformation mechanism. No concrete evidence for crazing was presented.

1.2. Toughening by shear flow and crazing

Bucknall and co-workers [18] proposed that massive crazing and shear flow are the two energy-absorbing mechanisms in rubber-modified plastics. They used tensile creep dilatometry to study these mechanisms in rubber-modified epoxies [10, 11]. In their analysis they assume that shear flow creates no volume change, whereas crazing does; therefore, the slope of the volume strain $\Delta V/V_0$ against longitudinal strain ε_l curve equals zero for a pure shear-flow process, and equals unity for a pure crazing process. Intermediate slopes would be produced by proportionate mixing of the two processes, i.e. a Rule of Mixtures was assumed. Using this type of technique they found that in rubber-modified epoxies volume strain increased with rubber content, as did fracture toughness, and they concluded that a combination of shear flow and massive crazing were the toughening mechanisms. They also showed an electron micrograph of a single craze in epoxy [11, 18]. However, other workers have found [14, 15, 19] that volume dilation cannot be unambiguously and exclusively attributed to crazing; voiding can also cause volume dilation [20]. These latter results indicate that other types of evidence for massive crazing must be presented to corroborate the volume strain data. In fact doubts as to the existence of crazes in a tightly cross-linked glassy polymer have been voiced by several authors [1, 2, 21, 22] despite reports of their having been observed [11, 23, 24]. As far as the toughening mechanism is concerned, the real question is not whether crazes exist in cross-linked glassy polymers, but how much they contribute to the toughness of these materials. Since Bucknall and co-workers [10, 11] did not present micrographic evidence to demonstrate the existence of massive crazing, its being a toughening mechanism for these epoxies is doubtful.

1.3. Rubber stretching and tearing

A quantitative model was recently advanced by Kunz [1] and Kunz-Douglass *et al.* [2] based on the idea that elastic energy stored in the rubber during stretching is dissipated irreversibly when the particles fail. This is the only model proposed thus far that attributes the toughness enhancement of rubber-modified epoxies entirely to the rubber particles. This quantitative model can account for an increase of a factor of two in the fracture toughness, which was the amount found by these authors. Unfortunately, others [3–11] have found increases that are an order of magnitude greater. The rubber-modified epoxies prepared by Kunz and co-workers [1, 2] achieved a level of toughness much lower than that obtained in the present investigation, as well as typical values reported in the literature. The discrepancy in the reported toughness values points out a common problem in these materials, i.e. the sensitivity of the material properties to the conditions of curing [25]. The work by Kunz and co-workers has perhaps quantified the order of magnitude of the contribution to toughness from the rubber particles alone. A recent publication by these workers [26] on low-temperature results continues to support their model.

1.4. Cavitation and plastic zone formation

Bascom and co-workers [3, 6–9] found that in rubber-modified epoxy adhesives, plastic zone sizes are directly related to the toughness. They proposed that cavitation caused by the triaxial tension ahead of the crack tip increases the size of the plastic zone and that plastic flow of the epoxy matrix and elongation of the particles also contribute to the toughness [3]. In agreement with Bascom and co-workers, Kinloch *et al.* [27] presented TEM and SEM micrographs to support the notion that cavitation and plastic shear yielding of the epoxy matrix are the microdeformation mechanisms occurring at the crack tip that dissipate energy and produce the toughening effect.

It is clear from the foregoing review that the issue of the toughening mechanism in elastomer-modified epoxies is far from settled – nearly every possible mechanism has been proposed and has found some support. The purpose of this work is to fill in some of the missing information and to elucidate the deformation mechanisms in these complex materials. The mechanical studies are reported in this part. Part 2 [28] contains the results of studies using various microscopy techniques. Part 3 [29] extends the studies to the effect of cross-link density.

2. Experimental procedure

2.1. Materials

The materials used in our investigation consisted of Epon 828, which is a liquid diglycidyl ether of bisphenol-A (DGEBA) produced by Shell Chemical Co. It was cured with piperidine, which was used as received (Aldrich Chemical Co.). The rubbers used were Hycar^R CTBN 1300X8, Hycar CTBN 1300X13 and Hycar CTBN 1300X15 produced by the B. F. Goodrich Chemical Co. These are liquid copolymers of butadiene and acrylonitrile with carboxyl end-groups. The manufacturer's published properties for these liquid rubbers are shown in Table I. Bisphenol-A (BPA), a resin-modifier used in these studies, was a reagent-grade solid 4-4′-isopropylidienediphenol from the Aldrich Chemical Co.

TABLE I Properties of Hycar CTBN rubbers

Property	Designation		
	1300X15	1300X8	1300X13
Viscosity, Brookfield (mPa sec) or cP at 27° C (81° F)	55000	125000	625000
Carboxyl content (%)	2.47	2.37	2.40
Molecular weight	3500	3500	3500
Functionality	1.9	1.85	1.85
Acrylonitrile content (%)	10	17	27
Solubility parameter	8.45	8.77	9.14
Heat loss, 2 h at 130° C (266° F) (%)	< 2.0	< 2.0	< 2.0
Specific gravity at 25° C (77° F)	0.924	0.948	0.960

TABLE II Notation for rubber-modified Epon 828*

Amount of BPA (phr)	Type of Hycar CTBN rubber	Amount of rubber (phr)	Designation	T_g (°C)†
0	–	0	828	84.2
0	1300X8	5	828-8(5)	–
0	1300X8	10	828-8(10)	85.6
0	1300X8	15	828-8(15)	–
0	1300X8	20	828-8(20)	87.5
0	1300X8	30	828-8(30)	82.4
0	1300X15	5	828-15(5)	–
0	1300X15	10	828-15(10)	84.2
0	1300X15	15	828-15(15)	–
0	1300X15	20	828-15(20)	89.4
0	1300X15	30	828-15(30)	86.1
0	1300X13	5	828-13(5)	–
24	–	0	828-BPA(24)	104.4
24	1300X8	5	828-BPA(24)-8(5)	100.6
24	1300X8	10	828-BPA(24)-8(10)	–
24	1300X8	15	828-BPA(24)-8(15)	97.6
24	1300X8	20	828-BPA(24)-8(20)	90.5

*5 phr (parts per hundred parts resin by weight) piperidine was used for all material.
†Determined by differential scanning calorimetry at 20° C min^{-1} from second heating.

The first set of materials investigated consisted of 100 parts Epon 828, 5 parts piperidine and 0, 5, 10, 15, 20 and 30 parts Hycar CTBN. The second set of materials consisted of 100 parts Epon 828, 24 parts BPA, 5 parts piperidine, and 0, 5, 10, 15, and 20 parts Hycar CTBN. These materials were cured at 120° C for 16 h in a Teflon^R-coated mould.

To designate the various rubber-modified materials the notation shown in Table II is adopted.

2.2. Fracture toughness measurements

In this investigation fracture toughness is measured in terms of the critical strain-energy release rate, G_{Ic}. These values are in turn calculated from critical stress-intensity factor (K_{Ic}) values using the relationship

$$G_{Ic} = K_{Ic}^2/E \quad (2)$$

where E is the Young's modulus experimentally determined in uniaxial tension. K_{Ic} values are determined using single-edge-notched (SEN) type specimens in a three-point bend (3PB) geometry using the relationship

$$K_{Ic} = Y\sigma_y a^{1/2} = Y\frac{6}{4}\frac{P_f S}{tw^2}a^{1/2}$$

where Y is a shape factor, σ_y is the stress at failure, a is the crack length, P_f is the load at failure, S is the length of the span, t is the specimen thickness and w is the specimen width. The shape factor Y has the form

$$Y = 1.93 - 3.07\left(\frac{a}{w}\right) + 14.53\left(\frac{a}{w}\right)^2 - 25.11\left(\frac{a}{w}\right)^3 + 25.8\left(\frac{a}{w}\right)^4$$

K_{Ic} is determined by performing a least-squares fit to a plot of σ_y against $a^{-1/2}$, and computing the slope of the line. These SEN–3PB specimens have the dimensions of 11 mm × 6 mm × 100 nm. Sharp cracks are initiated by tapping with a hammer on a razor blade which has been immersed in liquid nitrogen. This crack-initiation procedure results in very sharp cracks. The absence of plastic zones ahead of the initiated crack was verified in several samples by examining a thin section of the specimen between crossed polarizers. This technique is discussed in Part 2 of this series [28]. These specimens are tested on a screw-driven Instron machine at a crosshead rate of 2.12 mm sec^{-1} using a span of 66 mm. The load against time trace is recorded using a strip chart recorder. Initial crack lengths are measured from the fracture surfaces using an optical microscope. Initially, seven or more SEN–3PB specimens per material were tested to determine K_{Ic}. However, the relationship between σ_y and $a^{-1/2}$ was found to be very linear for both neat and elastomer-modified epoxies. The required minimum number of specimens was therefore reduced to four.

2.3. Uniaxial tensile dilatometry

The tensile dilatometry technique used in this investigation is modelled after that used by Bucknall and co-workers [18], except that a constant displacement rate, rather than constant load, was used. Parts of the present technique are described elsewhere [15]. Dog-bone shaped specimens having gauge-section dimensions of 12.7 mm width × 6.3 mm thickness × 60 mm length and overall length of ~ 150 mm were cut from cast epoxy plaques with a high-speed router and a steel template. Cut surfaces were polished with fine emery paper. From two to three specimens of each material were tested at each set of conditions. This small number of specimens was sufficient to establish unambiguous trends in behaviour for each material and each set of testing variables. A servohydraulic testing machine (either an Instron or an MTS machine) was used at rates up to 254 mm sec^{-1}. Two extensometers with the requisite sensitivity were used to measure the longitudinal and width strains. The thickness strain was assumed to be identical to the width strain. The load and the two displacements were simultaneously recorded into a four-channel digital oscilloscope with 12-bit (0.025%) resolution. This oscilloscope is also equipped with data-processing capabilities, so that the stress and the two strains and the volume strain were all directly calculated. These results were either recorded on to an X–Y plotter or stored on magnetic discs for later use. The volume strain $\Delta V/V_0$ is calculated using the formula

$$\frac{\Delta V}{V_0} = (1 + \varepsilon_l)(1 + \varepsilon_t)^2 - 1 \quad (3)$$

where ΔV is the change in volume, V_0 is the original volume, and ε_l and ε_t are the longitudinal and transverse engineering strains, respectively. The experiments were performed at constant displacement rates, which means that the strain rate was approximately constant only in the initial 1 to 2% region. This initial

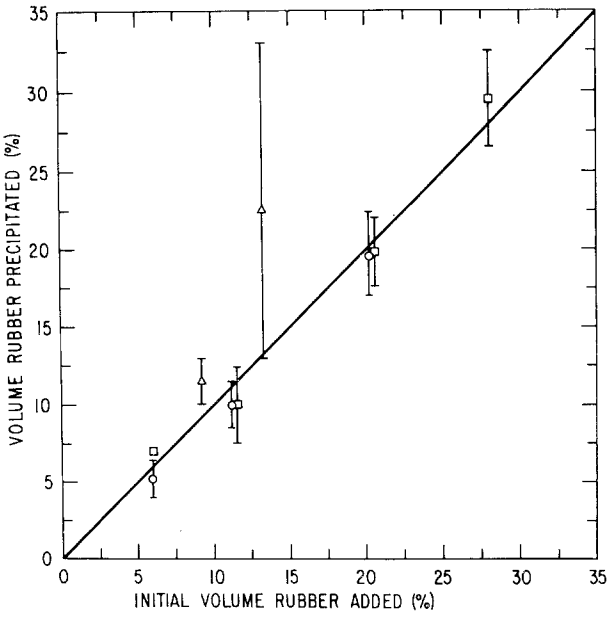

Figure 1 Initial volume percentage of rubber added against volume percentage of rubber precipitated as determined by transmission electronmicroscopy. (○) 828-8, (□) 828-15, (△) 828-BPA(24)-8.

value is reported here as the strain rate, $\dot{\varepsilon}$. The initial slopes of the stress–strain curves are reported here as the Young's modulus, E. The maximum in the engineering stress is reported here as the yield stress, σ_y. In those cases where the material formed a neck, i.e. at low rates, $\Delta V/V_0$ is reported only up to the yield strain, ε_y, which is defined as the strain where σ_y was reached. Indeed, one shortcoming of the present technique is that volume changes in a localized zone, such as in a neck, cannot be assessed.

3. Results and discussion

3.1. Morphology

Transmission Electron Microscopy (TEM) of osmium tetroxide (OsO_4) stained rubber-modified materials was performed to investigate the differences in morphology and determine the percentage of rubber volume [28]. Typically, the rubber particles appear to be a single phase without glassy occlusions, and with a sharp interface between the rubbery phase and the epoxy matrix. The 828-BPA-8(15) material (see Table II) is an exception in that it contains 2 to 10 μm rubber particles with a "salami-type" structure similar to that of rubber particles found in high-impact polystyrene, i.e. there are spherical glassy occlusions in the rubber particles. Fig. 1 is a plot of the initial volume percentage of rubber added against the volume percentage of rubber which has precipitated out, as measured by TEM. Typically, most of the CTBN precipitates out. However, the 828-BPA-8(15) material shows an apparent excess of precipitated CTBN due to epoxy occlusions in the largest rubber particles.

A quantitative analysis using the Schwartz–Saltykov method [31] on TEM micrographs containing a total of at least 86 rubber particles is performed to determine the rubber particle size distribution. Three types of rubber particle diameter distribution are found: (i) a nearly monodisperse distribution for all the 828-8 (5 to 20 phr) systems (1 to 2 μm) and for the 828-BPA(24)-8 (5 to 10 phr) systems ($\sim$0.5 μm); (ii) a polydisperse distribution for the 828-15 (5 to 30 phr) systems (1 to 10 μm); and (iii) a bimodal distribution for 828-BPA-8(15) (< 1 μm and 2 to 10 μm). The particle size distribution for the 828-15 series is shown in Fig. 2.

3.2. Fracture toughness

Figs 3 to 5 show that a linear relationship exists between σ_y and $a^{-1/2}$ for the neat resin as well as the elastomer-modified resins, including those with 30 phr elastomer. These results support the use of linear elastic fracture mechanics. Consequently, K_{Ic} may be easily converted to G_{Ic} by using the Young's modulus of each material. However, as tougher materials are tested ($G_{Ic} > 2\,kJ\,m^{-2}$) there is evidence – the load–deflection curves show a slight curvature – that G_{Ic} would be more accurately determined using an elastic energy type method.

The critical strain-energy release rate, G_{Ic}, is plotted against the rubber content for three rubber-toughened epoxies in Fig. 6. These toughness values are somewhat lower than those published by other investigators, perhaps because a higher degree of plane-strain constraint was achieved or simply because our initial cracks were sharper. These results show that fracture toughness is a strong function of rubber content, but not significantly dependent on the rubber particle size. The Hycar CTBN 1300X8 modified

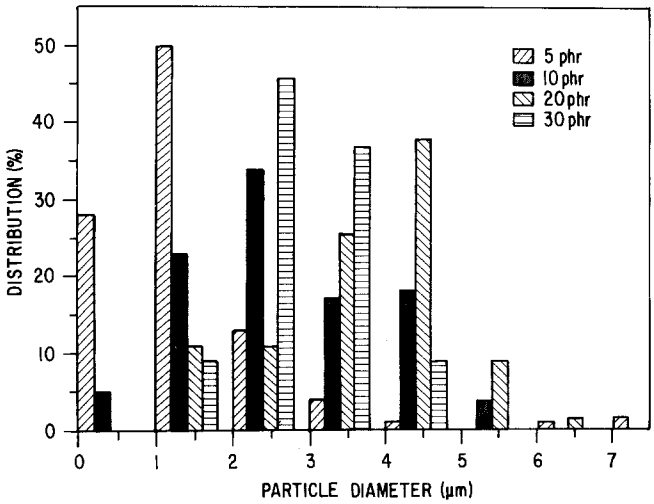

Figure 2 Particle size distribution for the 828-15 series of materials.

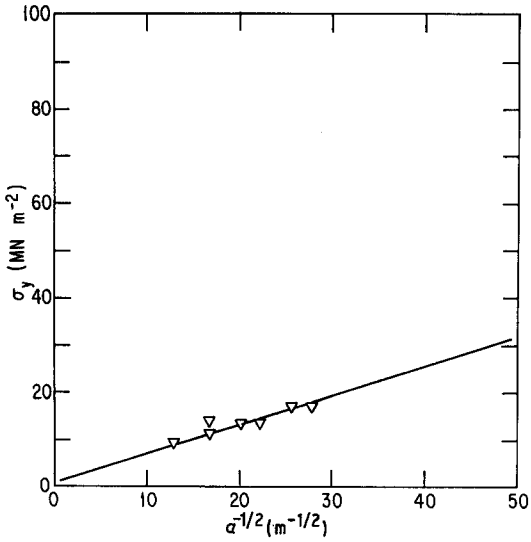

Figure 3 Dependence of failure stress σ_y on crack length a for Epon 828. $K_{Ic} = 0.63\,MN\,m^{-3/2}$.

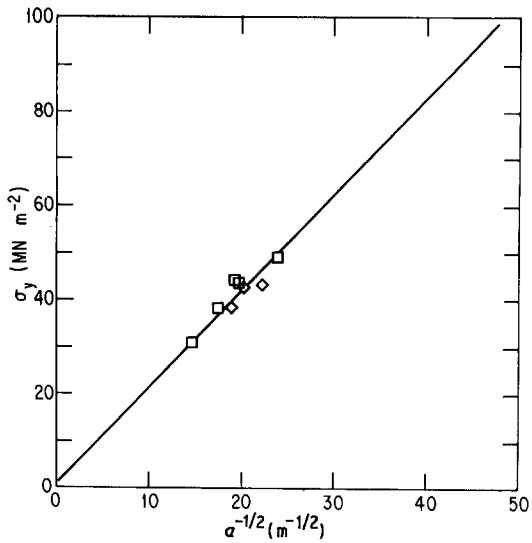

Figure 5 Dependence of failure stress σ_y on crack length a for 828-15(30). $K_{Ic} = 2.06\,MN\,m^{-3/2}$.

epoxies, containing $\sim 1\,\mu m$ diameter rubber particles, are not significantly tougher than the Hycar CTBN 1300X15 modified epoxies, which has ~ 5 to $10\,\mu m$ diameter rubber particles. The BPA-modified epoxies are even tougher than the previously mentioned epoxies at the 5 to 10 phr elastomer level, even though the particle diameters are submicrometre in size. We will attempt to show later that this is *not* a particle-size effect. It is important to note that the sizes of the stress-whitened zones formed in front of the starter cracks increase as G_{Ic} increases. The formation of these plastic zones results in enhanced toughness. The microscopic mechanisms which lead to these plastic zones are elucidated by tensile dilatometry.

3.3. Uniaxial tensile properties

Having shown that the epoxies prepared in these experiments are indeed toughened to a comparable extent to those reported in the literature, we now characterize their deformation behaviour in uniaxial tensile tests. The dependence of the tensile modulus on rubber content at $27 \pm 3°C$ is shown in Fig. 7. The approximately linear decrease of the moduli for the 828-8 and 828-15 series of materials is expected, and can be modelled quite well on a volume fraction basis by Kerner's equation, assuming a negligible modulus for the rubber. The large dispersion in the size of the rubber particles in these two series has no significant effect. The BPA-modified resin series has lower moduli in the composition range tested. At 15 phr rubber there is a more significant drop-off in the modulus because the rubber particle size distribution has become very broad, and the larger particles contain glassy occlusions.

The yield stress of the 828-8 series exhibits a linear decrease with rubber content (Fig. 8), as for the modulus. By comparison, the 828-15 series exhibits a more rapid initial drop-off. We interpret this to be due to the existence of large numbers of small rubber particles between the large ones in the latter series. At 20 phr the 828-15 material now has a relatively uniform distribution of particle size (Fig. 2); thus the yield stress becomes more consistent with that of the 828-8(15)

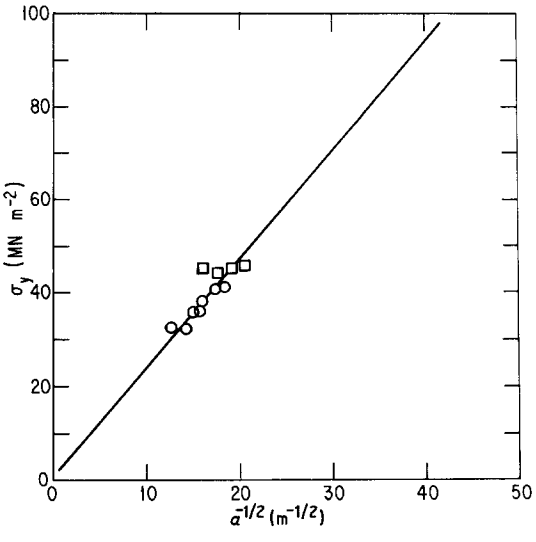

Figure 4 Dependence of failure stress σ_y on crack length a for 828-8(10). $K_{Ic} = 2.34\,MN\,m^{-3/2}$.

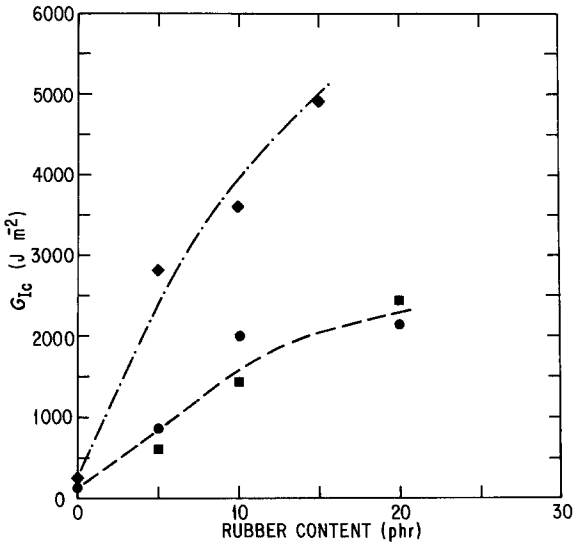

Figure 6 The strain-energy release rate G_{Ic} as functions of rubber content for three types of modifier: (●) 828-8, (■) 828-15, (◇) 828-BPA-8.

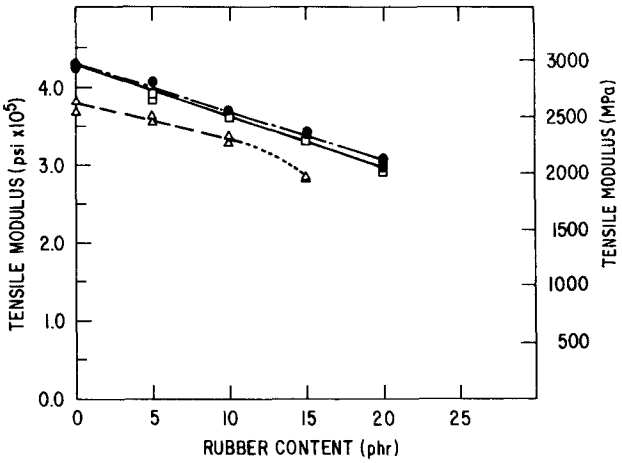

Figure 7 Dependence of tensile modulus on rubber content for three types of modifier: (●) 828-8, (□) 828-15. (△) 828-BPA(24)-8.

material. A similar argument can be made to explain the rapid drop-off of the yield strength of the BPA-modified series, again because at higher rubber content many small rubber particles exist between the large ones. Implicit in this interpretation is the assumption that the particles interact with each other, so that the effect of the particles is much more than that of simply replacing the matrix by a certain volume fraction of low-strength and low-modulus material. That such might be the case is further supported by the much faster decrease in the yield strength than in the modulus as rubber content increases.

The rubber particles interact in yet another manner: they apparently speed up the relaxation time of the composite. In Figs 9 to 11 the yield stresses of the 828-8, 828-15 and the 828-BPA(24)-8 series of epoxies are plotted against the logarithm of the strain rate. In the neat resin (828) the yield stress rises with increasing strain rate. We shall call this phenomenon "strain-

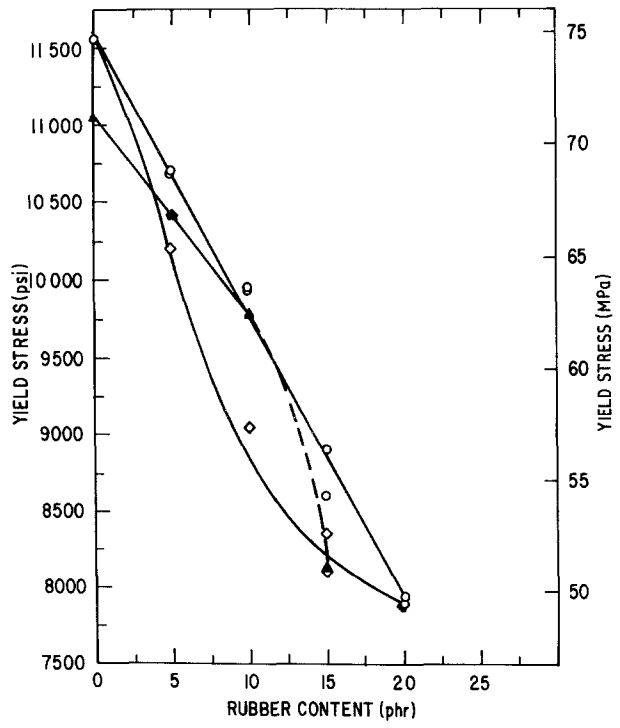

Figure 8 Dependence to tensile yield stress on rubber content for three types of modifier: (○) 828-8, (◇) 828-15, (▲) 828-BPA(24)-8.

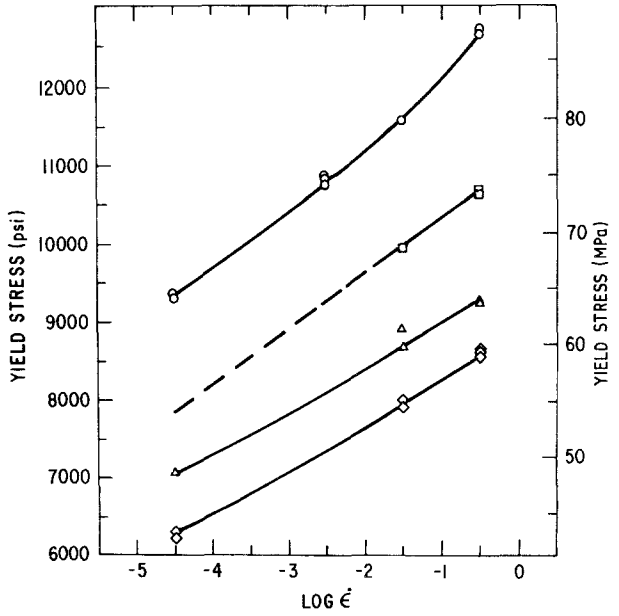

Figure 9 The effect of strain rate on the tensile yield stress of 828-8 materials: (○) 828, (□) 828-8(10), (△) 828-8(15), (◇) 828-8(20).

rate sensitivity". It comes about presumably because the stress required to accelerate the relaxation rate such that it matches the externally applied strain rate — which is when yielding occurs — must go up with the strain rate. As rubber particles are added, however, the strain-rate ($\dot{\varepsilon}$) sensitivity systematically decreases in all these series. Thus it appears that the composites are behaving as if the intrinsic relaxation rates are higher than in the neat resins. We now speculate on the cause of this phenomenon. As the composites are deformed, stress concentrations develop around the rubber particles. When the particles are sufficiently close to each other, the stress-concentration fields overlap. In the regions of overlap the relaxation rate is locally accelerated. This phenomenon of strain-accelerated relaxation has been noted elsewhere [30]. We shall show in a subsequent paper [28] that shear bands are indeed formed locally

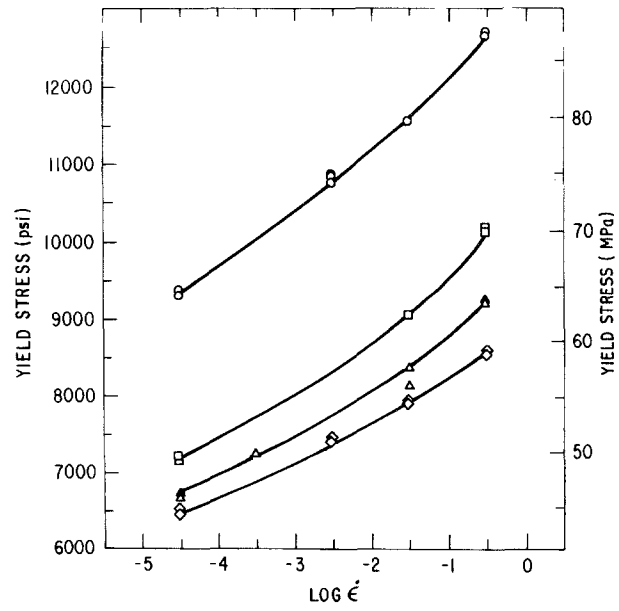

Figure 10 The effect of strain rate on the tensile yield stress of 828-15 materials: (○) 828, (□) 828-15(10), (△) 828-15(15), (◇) 828-15(20).

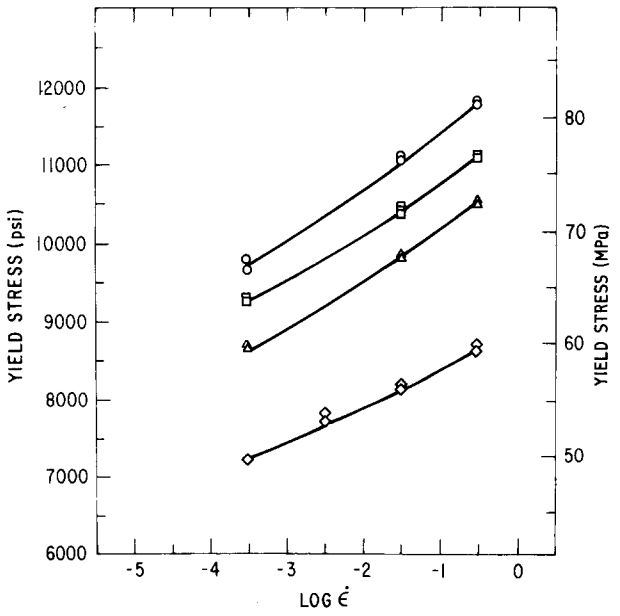

Figure 11 The effect of strain rate on the tensile yield stress of 828-BPA-8 materials: (○) 828-BPA(24), (□) 828-BPA(24)-8(5), (△) 828-BPA(24)-8(10), (◇) 828-BPA(24)-8(15).

between rubber particles in the directions where maximum shear-stress concentration overlap is expected to occur. These observations can be extended to predict that the tougher epoxies will also have ductile–brittle transitions at higher rates of deformation, and, equivalently, at lower temperatures.

Adding rubber particles has the expected effect, namely that both the Young's modulus and the nominal yield stress decrease with increasing rubber content; and increasing the rubber content does not significantly increase the elongation to break. By comparison, strain rate has a more significant effect on ductility. The modulus of the 828-BPA(24)-8 system deviates from linear dependence on rubber content. This is probably due to the significant difference in the morphology of the rubber particles, namely the existence of glassy inclusions. The yield stress of the 828-15 system also shows significant deviation from the linear dependence on rubber content, and is lower than the yield stress of the 828-8 system by ~5 to 10%, except at 20 phr rubber. Since the moduli of the two systems are very similar, the lowering of the yield stress must be due to additional non-linear processes that occur near yield. The broad distribution of particle sizes in this system, which results in small interstitial particles in between the larger particles in the 5, 10 and 15 phr systems, may be the cause for the reduction in yield stress. The effect of void size distribution on the yield and ductility of elastoplastic solids has been modelled [20, 32–34] with results that generally agree with the observations made here. The particle size distribution of the 828-15(20) system is more uniform; hence its yield stress is nearly the same as that of the 828-8(20) system, which also has a very uniform particle size distribution.

The well-known effect of strain rate on the yield stress is also observed in these experiments. The strain-rate dependence of the yield stress of the various materials can be described approximately as log–linear. The slight curvature could be due to a dispersion in the relaxation processes. In the rubber-modified systems, the rate dependence of the yield stress decreases as the rubber content goes up. This suggests that the relaxation rate in the matrix is accelerated [30].

3.4. Tensile dilatometry

Engineering stress–strain data were obtained simultaneously with volume-strain data during the uniaxial tensile dilatometry experiments. In the interest of brevity not all the stress–strain and volume-strain curves are presented in this paper; only those that represent typical effects of the variables are presented. To aid in the interpretation of the data obtained from these tests both stress–strain and volume-strain curves are presented in the same graphs.

Fig. 12 shows the yield and volume dilation behaviour of Epon 828 neat resin at various strain rates. At $\dot{\varepsilon} = 3.2 \times 10^{-5}\,\text{sec}^{-1}$, the pronounced maximum and subsequent drop in the nominal stress is impressive. From the amount of volume dilation (0.4%) and tensile strain at yield (4.2%), it can be

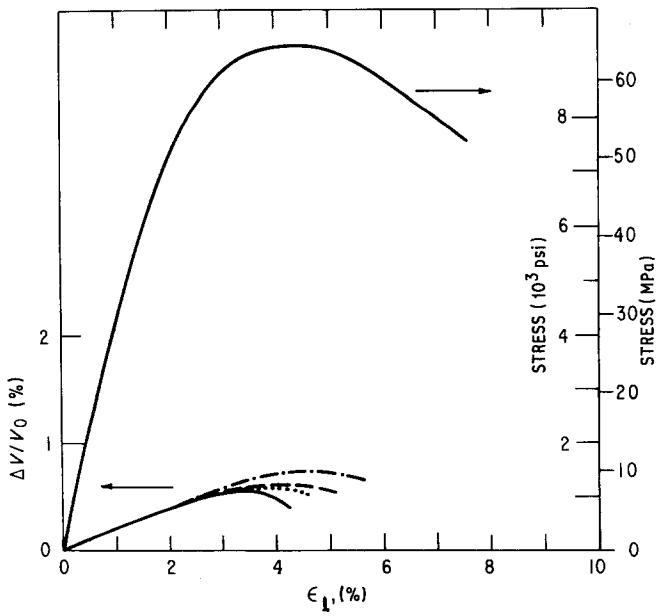

Figure 12 Upper curve: engineering stress–strain behaviour of Epon 828 at 27 ± 3° C and a strain rate of $3.2 \times 10^{-5}\,\text{sec}^{-1}$. Lower curves: dependence of volume strain on longitudinal strain at various strain rates; (——) 3.2×10^{-5}, (· · · ·) 3.2×10^{-3}, (– – –) 3.2×10^{-2}, (– · –) $3.2 \times 10^{-1}\,\text{sec}^{-1}$.

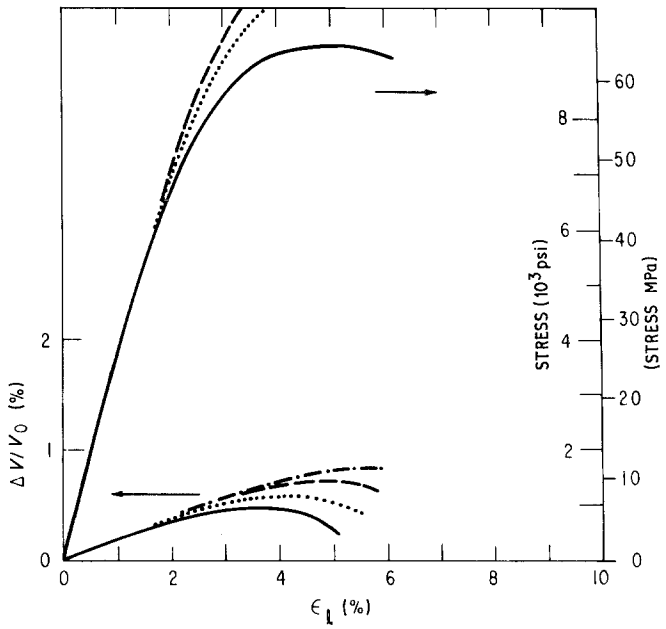

Figure 13 Upper curves: engineering stress–strain behaviour of 828-BPA at 27 ± 3° C and three strain rates; (– – –) 3.2×10^{-2}, (· · · ·) 3.2×10^{-3}, (——) 3.2×10^{-5} sec^{-1}. Lower curves: dependence of volume strain on longitudinal strain at various strain rates; (——) 3.2×10^{-5}, (· · · ·) 3.2×10^{-3}, (– – –) 3.2×10^{-2}, (– · –) 3.2×10^{-1} sec^{-1}.

calculated that the true yield stress is higher than the nominal stress by only approximately 3.8%. By assuming that the material deforms after the yield point at constant volume, the correction for true stress is only an additional ~3.3%, i.e. a total correction of 7.1% at rupture. Thus, the true stress behaviour also exhibits a pronounced intrinsic strain-softening effect. Visual inspection during the tests indicates that in the neat resin, shear-band formation occurs after the load drop. This observation is in agreement with the behaviour of the volume-strain curves, which are discussed in the next paragraph, where the levelling off and subsequent decrease of the $\Delta\dot{V}/V_0$ curve is interpreted to be the result of shear-band formation.

Fig. 12 also shows a plot of volume strain ($\Delta V/V_0$) against elongational strain (ε_1) at 27 ± 3° C for several strain rates. The initial, approximately linear, portion of these curves is due to homogeneous deformation with a constant lateral contraction ratio, i.e. a constant rate of dilation. Before the yield stress is reached, $\Delta V/V_0$ exhibits a maximum, followed by a subsequent decrease. This maximum signifies the onset of the shear-flow process. Note that the apparent volume decrease is mostly an artefact due to the inability of the extensometers to measure strains when localized shear-banding occurs. The curves plotted here are terminated at the strain where gross necking takes place. The effect of increasing strain rates is one of delaying and increasing the $\Delta V/V_0$ maximum in a manner similar to its effect on the yield stress. In other words, at increasingly high strain rates the shear-flow process is retarded.

The tensile dilatometry data of the BPA-modified Epon 828 neat resin is shown in Fig. 13. By comparison with Epon 828, this material has a lower modulus, reaches the maximum in the nominal stress at a slightly higher strain, and exhibits a less pronounced intrinsic softening. Shear bands were also observed in the fractured tensile specimens. Again, the effect of increasing the strain rate is to delay the departure from linearity in *both* the stress and the volume strain. The deviation from linearity in the stress–strain curves is clearly due to the onset of a shear-flow process even before the maximum in stress is reached. It is interesting to note that the shear-flow process in this material is more severely retarded by increasing strain rates than in Epon 828.

We now turn to the epoxies toughened by 10 μm diameter rubber particles (828-15 materials) and examine the effects of strain rate and rubber content. Fig. 14 is a plot of the tensile dilatometry data taken at 27 ± 3° C with varying rubber content. The volume-strain curves show an initial constant $\Delta\dot{V}/V_0$ portion followed by an increasing $\Delta\dot{V}/V_0$ portion which is indicative of a voiding process. These are then followed by decreasing $\Delta\dot{V}/V_0$, signifying the onset of the shear-flow process. Increasing rubber content delays the onset of the voiding process. The effect of strain rate on $\Delta V/V_0$ of the 828-15(20) material is shown in Fig. 15. Again, high strain rates delay the shear-flow process and promote voiding.

The effects of strain rate and rubber content on the deformation of the epoxies toughened by ~1 μm rubber particles (828-8 materials) were also studied by tensile dilatometry. Fig. 16 contains a plot of stress and $\Delta\dot{V}/V_0$ against ε_1 at 27 ± 3° C with varying rubber content. The curves again show an initial constant $\Delta\dot{V}/V_0$ portion and, by comparison with Fig. 12, some signs of voiding. In this case, however, the amount of voiding does not increase with rubber content as it does in the 828-15 system. The 828-8(20) material shows evidence for enhanced shear flow at low ε_1. The apparent lack of dependence of the volume strain on rubber content is evidently due to the low strain rate. The effect of strain rate on the 828-8(20) material is shown in Fig. 17. Here increasing strain rates are shown to retard the shear-flow process and promote voiding. This behaviour points out the difficulty in attempting to determine the deformation mechanism during impact by using low strain-rate tests [15].

The epoxies toughened with both BPA and CTBN rubber were also studied using the same tensile dilatometry technique. Fig. 18 contains a plot of $\Delta V/V_0$ against ε_1 at 25 ± 3° C with varying rubber content.

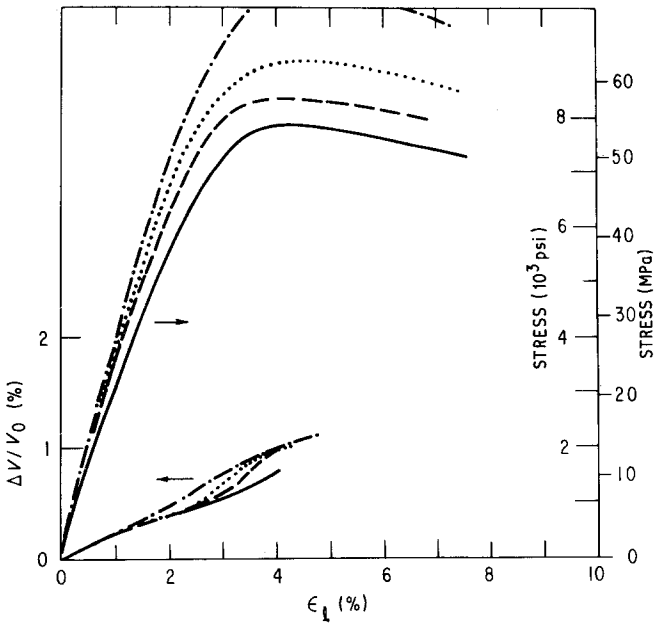

Figure 14 Upper curves: engineering stress–strain behaviour of 828-15 at various levels of rubber content; (– · –) 5, (· · · ·) 10,. (– – –) 15, (——) 20 phr. Lower curves: effect of rubber content on volume strain. Strain rate $3.2 \times 10^{-2}\,sec^{-1}$, temperature 27 ± 3° C.

At 5 and 10 phr rubber the $\Delta V/V_0$ curves show a constant $\Delta \dot{V}/V_0$ portion and then the onset of the shear-flow process. At 15 phr the $\Delta V/V_0$ curve indicates a slight voiding process because beyond $\varepsilon_1 = 3\%$ it exhibits only a constant $\Delta \dot{V}/V_0$ behaviour. The effect of strain rate on the volume-dilation behaviour of the latter material is shown in Fig. 19. Two distinct types of behaviour are noted. At low rates the material behaves as if the rubbery phase were not present, but at high rates voiding takes place where shear-banding would have occurred at the lower rates. It is evident that the shear process is very rate-sensitive in this material.

Increasing the rubber content invariably promotes either homogenous or localized shear. Subsequent behaviour depends on the strain rate. It appears that increasing the rubber content also increases the maximum volume strain at high rates. This is confirmed by SEM micrographs, to be shown in a separate paper [28]. These results also suggest that particle–particle interaction increases with rubber content.

In most cases the effect of strain rate on the mode of deformation is surprisingly significant. At low rates the volume-strain behaviour of some of the rubber-modified materials appears to be no different to that of the neat resin. The accelerated voiding process is evident only at higher rates. The voiding region is sometimes followed by a region of decreasing volume-strain rate. This is strongly indicative of shear localization promoted by the presence of numerous voids. The effect of strain rate on the neat resins demonstrates that the shear-flow process is retarded by high rates. When rubber particles are added the ability of the matrix to form shear bands is enhanced by these stress concentrators. However, as inhomogeneous shear deformation becomes increasingly difficult with high rates, the hydrostatic tensile stress component is unrelieved. At this point, either interfacial failure between the rubber and the matrix or cohesive failure in the matrix or the rubber itself has to take place, resulting in increasing volume strain. SEM micrographs [28] give conclusive evidence that the hydrostatic tensile stress is relieved by cavitation and fracture of the rubber particles.

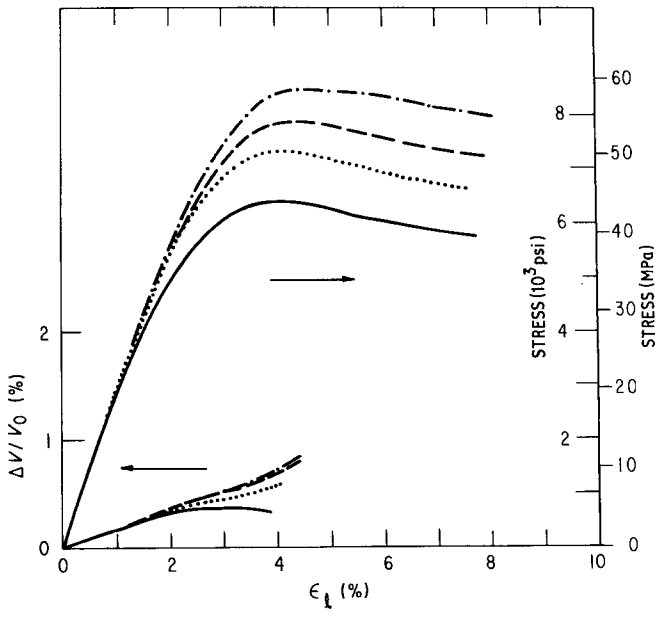

Figure 15 Upper curves: engineering stress–strain behaviour of 828-15(20) at various strain rates; (——) 3.2×10^{-5}. (· · · ·) 3.2×10^{-3}, (– – –) 3.2×10^{-2}, (– · –) $3.2 \times 10^{-1}\,sec^{-1}$. Lower curves: effect of strain rate on the volume strain behaviour. Temperature 27 ± 3° C.

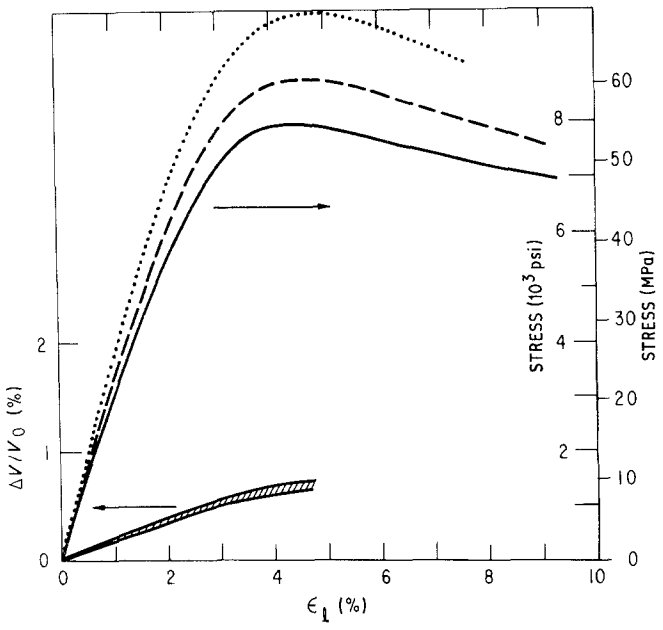

Figure 16 As in Fig. 14, but for the 828-8 system; (· · · ·) 10, (– – –) 15, (——) 20 phr. At this strain rate, the dependence of the volume strain on the rubber content is insignificant.

4. Summary and conclusions

With the exception of the 828-13 system, the rubber-modified epoxies have been shown to be toughened over the neat resins by over an order of magnitude. The toughening effect is made possible by the formation of a two-phase system, the rubber having precipitated out of the mixture during the polymerization process. The difference in the solubility due to acrylonitrile content causes the rubber to precipitate out into spherical particles with diameters ranging between 0.1 and 10 μm. The toughness is found to be primarily a function of rubber content. The effect of rubber particle size is, on the whole, not significant. On the other hand, the BPA-modified matrix, which has a slightly lower modulus and yield stress, produces a significant increases in toughness when rubber-modified. At room temperature and above, the uniaxial stress–strain behaviour of the neat resins exhibits a surprising amount of ductility. These materials yield with a maximum in the true stress, followed by intrinsic strain-softening. The strain-softening is caused by the formation of shear bands. The localization of the shear deformation causes the volume strain to exhibit a maximum. This maximum occurs at increasingly high strains as the strain rate increases. The retardation of the shear localization process by increasing strain rates is undoubtedly an important factor in the brittleness of the neat resins in crack propagation. While the shear localization process is retarded, the volume strain increases. The bulk strain energy increases roughly as the square of the volume strain, so the inability of the shear localization process to take place exacts a penalty in the building up of bulk energy. Thus, any mechanism that facilitates the shear-localization process, or, alternatively, dissipates the bulk strain energy, would enhance the toughness. The rubber particles appear to do both.

The tensile volume-dilation behaviour of the two-phase rubber-modified epoxies appears to be very similar to those of the neat resins at low rates. The rubber particles definitely enhance the shear localization

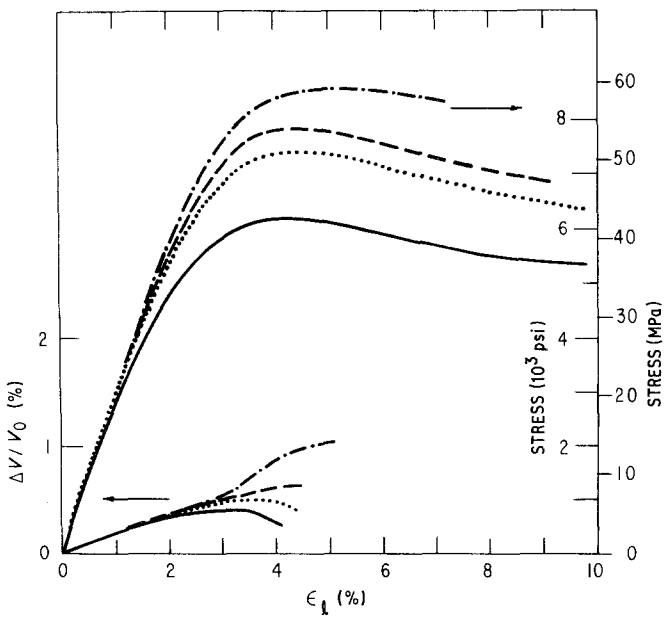

Figure 17 As in Fig. 15, but for the 828-8(20) material; (——) 3.2×10^{-5}, (· · · ·) 3.2×10^{-3}, (– – –) 3.2×10^{-2}, (– · –) 3.2×10^{-1} sec^{-1}.

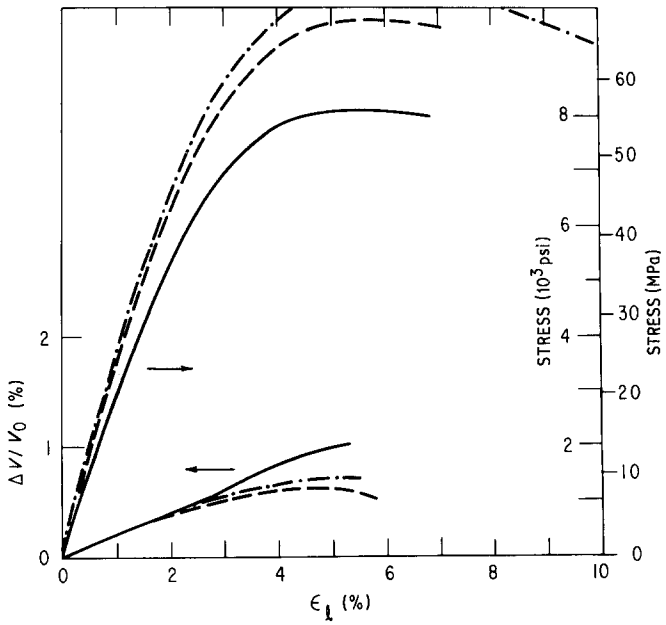

Figure 18 As in Fig. 14, but for the 828-BPA(24)-8 system; (–·–) 5, (– – –) 10, (——) 15 phr.

process, as evidenced by the maximum in the volume strain following Poisson's-effect dilation. At sufficiently high rates, however, when the neat resins typically dilate at a nearly constant rate almost up to the yield point, the rubber particles cause the material to expand to a higher rate than the neat resin. In a separate paper [28] micrographs will be presented that will show that this expansion is caused by cavitation of the rubber particles. The cavitation is followed by the onset of the shear localization process, which would not have taken place in the neat resin under the same conditions. Thus, the rubber particles dissipate the bulk strain energy by cavitation; and, at the same time, the shear-strain energy is allowed to build up to the point where shear yielding can take place. The voids left behind by the cavitated rubber particles act further as stress concentrators. Theoretical model calculations show that they reduce the octahedral shear stress to yield [32] and they grow and promote the formation of plastic zones between voids [20]. Shear-band formation is enhanced in such a voidy solid [33, 34]. All these theoretical predictions are consistent in the main with the observations made here.

In the fracture of these materials containing sharp cracks, the stress configuration is somewhat different from the tensile case. A zone of high hydrostatic tension exists ahead of the crack tip. The hydrostatic tension causes rapid cavitation of the rubber and growth of the resultant voids, micrographic evidence for which will be shown in a separate paper [28]. In the tensile dilatometric studies, cavitation of the rubber occurs at a tensile strain of ~ 2 to 3%, and the maximum additional volume strain caused by the cavitation is but a fraction of one per cent. In any case, it is reasonable to extrapolate from the tensile dilatometry results that, in the case of crack propagation, a zone of voids and shear bands is formed ahead of the crack tip as soon as stress is applied to open up the crack faces. This voided zone blunts the crack, causing it to behave as if it had a much larger crack-tip radius. This blunt crack, upon the application of further tension, causes an even larger plastic zone to form. Thus, a large volume of material above and below the crack plane is caused to undergo plastic deformation. It is the creation of this plastic zone that is the principal toughening mechanism. The crack, in the meantime,

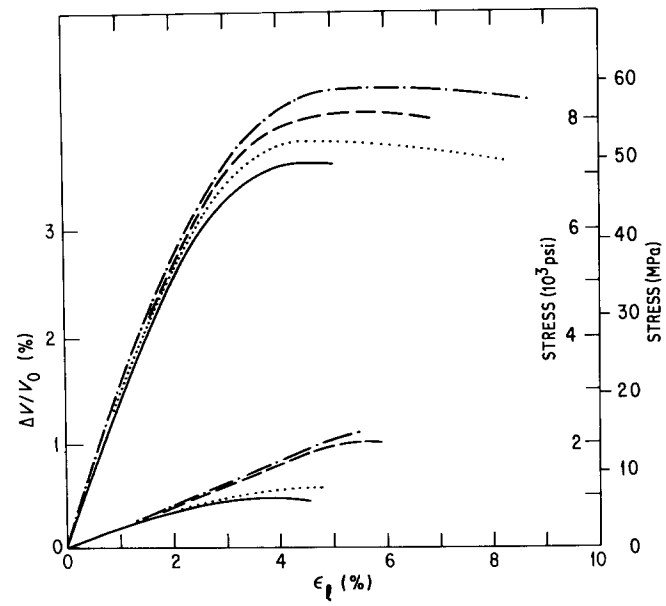

Figure 19 As in Fig. 15, but for the 828-BPA(24)-8(15) material; (——) 3.2×10^{-4}, (····) 3.2×10^{-3}, (– – –) 3.2×10^{-2}, (–·–) 3.2×10^{-1} sec^{-1}.

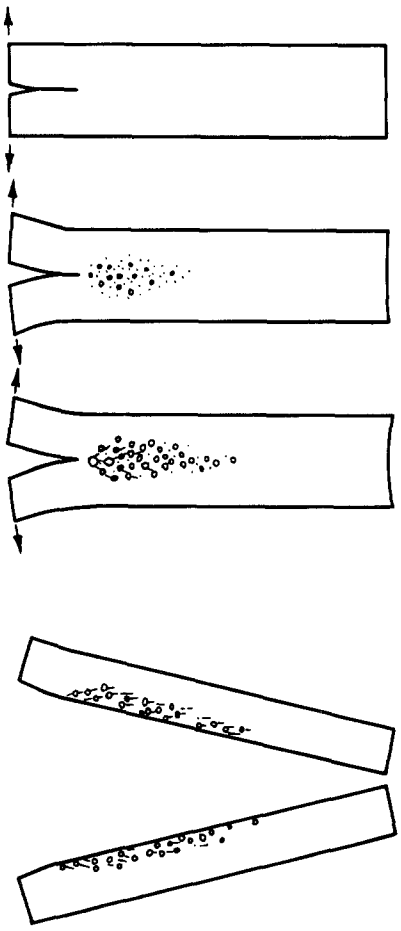

Figure 20 A schematic representation of the deformation processes ahead of a crack tip. From top to bottom: a crack is subjected to a load in the opening mode; increasing displacement and load causes the rubber particles in a zone ahead of the crack tip to cavitate; on further loading, cavities grow larger, with those at highest stress levels initiating shear bands; finally, if the strain energy continues to increase, the critical level is reached and unstable (fast) fracture occurs.

propagates through the voided plane when the ligaments between the voids can no longer support the tensile stress. The fracture process described above is schematically depicted in Fig. 20.

The proposal advanced here, that plastic zone formation is the principal toughening mechanism, finds support also in the work by Bascom and Cottington [7] on the fracture toughness of rubber-modified epoxy adhesive joints. These workers found that the fracture toughness of epoxy adhesive joints is strongly dependent on the thickness of the joint. When the joint thickness is too small, the fracture toughness is low. Maximum toughness is attained when the joint thickness is about the same as the height of the plastic zone.

The rubber particles appear to play an important role. They first enhance shear localization by acting as stress concentrators. Then, as bulk strain energy increases, cavitation takes over and dissipates the energy, making further shear localization possible. Although the different types of rubber produce particles of different sizes, distributions and internal structures, the role played by them appears to be quite similar. No major effects due to particle size differences have been observed. This result contradicts the conclusions of Sultan and McGarry [5], but it should be pointed out that the smallest rubber particles they studied were 0.040 μm in diameter, much smaller than those studied here. The 828-BPA(24)-8(15) system, which has a bimodal distribution in rubber particle sizes, shows high toughness; but the supposed extra toughness enhancement due to bimodal size distribution, most recently studied by Bascom *et al.* [9], is not conclusively demonstrated here.

The dilatometric results show no evidence that massive crazing, which exists as a toughening mechanism in some thermoplastics, exists. These results contradict the conclusion of Bucknall and Yoshii [10], Sultan and McGarry [5] and Riew and co-workers [12, 13]. It should be emphasized that the possibility of crazing in cross-linked epoxies cannot be completely discounted by the present work. Based on available evidence, crazing is not an important energy-dissipation mechanism in the toughening of these epoxies.

In a subsequent paper [28] the nature of the plastic zone at the crack tip is examined using several microscopy techniques. The effect of cross-link density on ductility and toughenability of elastomer-modified epoxies will be examined in another future paper [29].

Acknowledgements

The authors wish to acknowledge the generosity of Dr K. Riew of B. F. Goodrich Co. for providing the liquid rubbers and a plaque mould free of charge. Mr C. Lizak kindly provided first-hand information on the preparation of the epoxy plaques. The authors also wish to thank Dr S. Kunz of Sandia Laboratories for providing copies of her PhD thesis. The authors are indebted to numerous scientists at the General Electric Research and Development Center for technical assistance and illuminating discussions. Dr C. B. Bucknall of the Cranfield Institute of Technology generously gave of his invaluable experience and advice. Finally, the authors wish to thank Dr N. Johnston of NASA–Langley, the Contract Monitor of this work, for his encouragement. This work was partially funded by NASA Contract No. NASI-16132.

References

1. S. KUNZ, PhD thesis, University of Cambridge (1978).
2. S. KUNZ-DOUGLASS, P. W. R. BEAUMONT and M. F. ASHBY, *J. Mater. Sci.* **15** (1980) 1109.
3. W. D. BASCOM and D. L. HUNSTON, in Proceedings of International Conference on Toughening of Plastics, London, 1978 (Plastics and Rubber Institute) p. 22.1.
4. J. N. SULTAN, R. C. LAIBLE and F. J. MCGARRY, *Appl. Polym. Symp.* **16** (1971) 127.
5. J. N. SULTAN and F. J. MCGARRY, *J. Polym. Sci.* **13** (1973) 29.
6. W. D. BASCOM, R. L. COTTINGTON, R. L. JONES and P. PEYSER, *J. Appl. Polym. Sci.* **19** (1975) 2545.
7. W. D. BASCOM and R. L. COTTINGTON, *J. Adhesion* **7** (1976) 333.
8. W. D. BASCOM, R. L. COTTINGTON and C. O. TIMMONS, *Appl. Polym. Symp.* **32** (1977) 165.
9. W. D. BASCOM, R. Y. TING, R. J. MOULTON, C. K. RIEW and A. R. SIEBERT, *J. Mater. Sci.* **16** (1981) 2657.
10. C. B. BUCKNALL and T. YOSHII, *Br. Polym. J.* **10** (1978) 53.
11. *Idem*, in Proceedings of 3rd International Conference on

Deformation, Yield and Fracture of Polymers, Cambridge, 1976 (Plastics and Rubber Institute) p. 13.1.
12. C. K. RIEW, E. H. ROWE and A. R. SIEBERT, *ACS Adv. Chem. Ser.* **154** (1976) 326.
13. E. H. ROWE, in Proceedings of International Conference on Toughening Plastics, London, 1978 (Plastics and Rubber Institute) p. 23.1.
14. H. BREUER, F. HAAF and J. STABENOW, *J. Macromol. Sci. Phys.* **B14** (3) (1977) 387.
15. M. A. MAXWELL and A. F. YEE, *Polym. Eng. Sci.* **21** (1981) 205.
16. A. F. YEE, W. V. OLSZEWSKI and S. MILLER, *ACS Adv. Chem. Ser.* **154** (1976) 97.
17. S. S. STERNSTEIN and L. ONGCHIN, *ACS Polym. Prep.* **10**(2) (1969) 1117.
18. C. B. BUCKNALL, "Toughened Plastics" (Applied Science, London, 1977).
19. R. RAMSTEINER, *Polymer* **20** (1979) 839.
20. A. NEEDLEMAN, *J. Appl. Mech., Trans. ASME* **39** (1972) 964.
21. J. MIJOVIK and J. A. KOUTSKY, *Polymer* **20** (1979) 1095.
22. R. J. YOUNG, in "Developments in Polymer Fracture-1", edited by E. H. Andrews (Applied Science, London, 1979) p. 183.
23. J. LILLEY and D. G. HOLLOWAY, *Phil. Mag.* **28** (1973) 215.
24. R. J. MORGAN and J. E. O'NEAL, in "Chemistry and Properties of Crosslinked Polymers", edited by S. S. Labana (Academic Press, New York, 1977) p. 289.
25. A. C. MEEKS, *Polymer* **15** (1974) 675.
26. S. C. KUNZ and P. W. R. BEAUMONT, *J. Mater. Sci.* **16** (1981) 3141.
27. A. J. KINLOCH, S. J. SHAW, D. A. TOD and D. L. HUNSTON, *Polymer* **24** (1983) 1341.
28. R. A. PEARSON and A. F. YEE, *J. Mater. Sci.* **21** (1986) 2475.
29. *Idem,* in preparation.
30. A. F. YEE, R. J. BANKERT, K. L. NGAI and R. W. RENDELL, in preparation.
31. E. E. UNDERWOOD, "Quantitative Sterology" (Addison-Wesley, Reading, Massachusetts, 1970) p. 109.
32. A. L. GURSON, *J. Eng. Mater. Tech., Trans. ASME* **99** (1977) 2.
33. H. YAMAMOTO, *Int. J. Fracture* **14** (1978) 347.
34. V. TVERGAARD, *ibid.* **17** (1981) 389.

Received 29 July
and accepted 18 September 1985